Stochastic Differential Scanning Calorimetry by Nonlinear Optical Microscopy

Alex M. Sherman[†], Andreas C. Geiger[†], Casey J. Smith[†], Lynne S. Taylor[‡], Jeremy Hinds[§], Paul A. Stroud[§], and Garth J. Simpson*[,†]

[†]Department of Chemistry, Purdue University, 560 Oval Drive, West Lafayette, Indiana 47907, United States

[‡]Department of Industrial and Physical Pharmacy, Purdue University, 575 Stadium Mall Drive, West Lafayette, Indiana 47907, United States

[§]Eli Lilly & Company, 1200 W. Morris Street, Indianapolis, IN 46221, United States

ABSTRACT: Stochastic phase transformations within individual crystalline particles were recorded by integration of second harmonic generation (SHG) imaging with differential scanning calorimetry (DSC). The SHG-activity of a crystal is highly sensitive to the specific molecular packing arrangement within a noncentrosymmetric lattice, providing access to information otherwise unavailable by conventional imaging approaches. Consequently, lattice transformations associated with dehydration/desolvation events were readily observed by SHG imaging and directly correlated to the phase transformations detected by the DSC measurements. Following studies of a model system (urea), stochastic differential scanning calorimetry (SDSC) was performed on trehalose dihydrate, which has a more complex phase behavior. From these measurements, SDSC revealed a broad diversity of single-particle thermal trajectories and direct evidence of a "cold phase transformation" process not observable by the DSC measurements alone.

In pharmaceutical drug development, drug substances and formulations with long-term physical and chemical stability ensure full optimized of a drug when administered to the patient. During the time consuming process of formulations development (estimated >3 months and $1 million) it is thus critical to employ methods that inform on possible avenues of reduced bioavailability.[1] Identifying possible failure points early can reduce the changes of late-stage failure, which can be costly and time consuming to remediate. For active pharmaceutical ingredients administered as crystalline formulations, phase transitions to alternate crystal forms can have deleterious effects on aqueous dissolution rates, affecting both oral and parenteral bioavailability.[2-4] Administering these drugs as amorphous solid dispersions or as liquid formulations does not altogether avoid the problem, as spontaneous crystallization can occur during storage or even *in vivo* under certain conditions.[5-11] Phase transitions can dictate both direct physical depletion of bioavailable drugs through transitions to non-soluble crystal forms, as well as susceptibility to chemical depletion through transitions to more reactive crystalline, liquid or glassy states. There is therefore a need in the pharmaceutical industry to thoroughly map the phase space of potential drug candidates, excipients, and mixtures.

Several thermal methods exist for characterizing phase transitions within pharmaceutical powders. Differential thermal analysis applies equal heat to reference and sample pans and measures the temperature differential between the two pans to detect thermal events associated with phase transitions. Thermal gravimetric analysis (TGA) continuously measures the mass of a sample while varying temperature. TGA is especially useful for dehydration and decomposition. Differential scanning calorimetry (DSC) enables the detection of phase transitions as a function of the energy differential between reference and sample pans heated to the same temperature. DSC is a widely used technique for phase transition characterization because of its sensitivity, ease-of-use, and short measurement time.[12]

Despite these advantages, DSC probes the energy transfer into the full ensemble of the sample, averaging over all particles in the formulation. Phase transitions for ensembles of crystals are predicted to be stochastic, with nucleation typically being the rate-limiting step on a per-particle basis.[13-15] If phase transformation is stochastic, individual transient events may be obscured or missed in ensemble-averaged analysis. Additionally, single-particle measurements can enable the accurate modelling of kinetics for phase transitions, allowing the distinction between different mechanisms of transition (i.e., concerted or continuous).[16]

Optical microscopy measurements of changes in gross morphology coupled with DSC can recover information on single-particle phase transformations. Reading and coworkers have developed an image analysis algorithm dubbed thermal analysis by structural characterization (TASC) to detect phase transitions and the spatial distribution of phases from images acquired using hot-stage microscopy.[17-21] TASC measures the subtle difference between an original image and subsequent images to quantify morphological changes within a region-of-interest as temperature is varied. The algorithm also accounts for the possibility of translation of the region-of-interest within the field-of-view (FoV). TASC is a fast and inexpensive method for characterizing the spatial distribution of phase transformations. However, TASC methods rely exclusively on morphological changes in the optical response, which are only intrinsically related to a subset of all possible phase transformations. Solid / solid phase transformations are largely inaccessibly by TASC, and glass / solid phase transformations can be challenging to reliably detect without perturbing the sam-

ple. Desolvation (including dehydration) or polymorph transitions in the solid state are typically not accompanied by obvious changes in the gross morphology of a particle but can profoundly influence physico-chemical characteristics that are accompanied by thermal transients in DSC measurements. In addition, structural re-arrangements between polymorphs with similar bulk free energies are quite challenging to detect by either conventional DSC or bright-field microscopy. Coupling DSC with concurrent imaging capabilities that are more directly tied to crystal form would help address these ambiguities associated with conventional bright-field microscopy and DSC.

In this work, we demonstrated the integration of second harmonic generation (SHG) microscopy with DSC analysis to monitor phase transitions on a per-particle basis. This multimodal approach enabled simultaneous single-particle analysis for distinguishing the impact of crystal size and shape on phase transitions in a single experiment, complementing the ensemble-averaged information obtained from DSC. Furthermore, the strict symmetry requirements for SHG allow the mapping of complex desolvation and crystal form transitions with sensitivity in the ppm regime.[22] Previous work has utilized the exquisite sensitivity of SHG microscopy to internal structure of the lattice in non-centrosymmetric crystals as a standalone tool for polymorph discrimination, calibration-free quantification of trace crystallinity, and protein crystal centering at X-ray beamlines.[23-25] Raman spectroscopy, terahertz spectroscopy, and SHG have all previously been used to characterize crystallinity, polymorphism, and phase transitions.[26-33] The merits of integrated SHG and DSC measurements are explored for a model system to then explore the complex phase transitions in trehalose dihydrate.

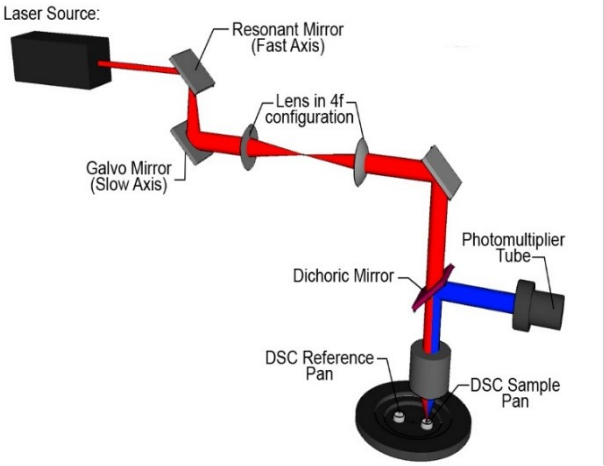

Figure 1. Schematic of the integrated SHG-DSC microscope. A pulsed laser beam (800 nm, 80 MHz) was scanned with a galvo-resonant scan pair, which was 4f coupled to the back of an objective and focused onto a DSC sample pan. The SHG signal was collected in the epi direction, isolated with a dichroic mirror and detected with a photomultiplier tube.

METHODS

SHG microscopy

The experimental apparatus is depicted in **Figure 1** and consists of a home-built SHG microscope integrated with an optical DSC stage (Linkam, DSC450). A tunable 80 MHz, Ti:sapphire, femtosecond laser (Spectra-Physics, Mai Tai) was used for the incident light source. The fundamental beam was raster-scanned across the sample using a resonant scanning mirror at 8.8 kHz (EOPC) for the fast-scan axis and a galvanometer mirror (Cambridge-Tech) for the slow-scan axis. A 4x, 0.1 NA objective (Nikon) was used to focus the beam onto the sample, and the SHG signal was collected in the epi direction through the same objective used for delivery of the fundamental beam. The laser was tuned to 800 nm with a power of 80–120 mW at the sample. Two long-pass dichroic mirrors (Chroma, 650DCXR) and a band-pass filter (Chroma HQ400/20M-2P) were used to isolate the 400 nm SHG signal before it was detected by a photomultiplier tube (PMT) (Hamamatsu, H7422P-40 MOD). Responses of the PMT were digitized synchronously with the laser pulses by using a digital oscilloscope card (Alazar Tech, ATS9350) and mapped onto 512 × 512 images via custom software written in-house (MATLAB).[34] The SHG videos were recorded at 17 frames per second for urea samples and at eight frames per second for trehalose samples.

DSC measurements

Stochastic differential scanning calorimetry (SDSC) measurements were acquired by integration of the home-built SHG microscope with a Linkam Optical DSC450 stage. The DSC temperature ramp range was 125–145 °C for the urea samples and 80–250 °C for the trehalose samples with ramp rates of 10 °C/min and 20 °C/min, respectively. Before the data collection, an isothermal hold time of two minutes for both urea and trehalose ensured a reliable starting temperature for all experiments to reduce the effects of initial temperature variation. Temperature and input power were measured by the DSC at a rate of five Hz. Standard aluminum sample pans were used in all DSC experiments, and were not sealed to allow for optical access of the sample. The DSC was calibrated using an indium standard in an open pan.

Data analysis

ImageJ (NIH) was used to perform single-particle analysis on the images acquired with the integrated SHG-DSC microscope. The single-particle SHG areas were measured by calculating the fraction of pixels above a threshold within the region of interest.

Sample preparation

Supersaturated solutions of urea (Sigma-Aldrich) were prepared in DI water solution and rapidly recrystallized in an ice bath. The water was decanted, and the crystals were left to dry overnight. Crystals were then passed through a 63 μm mesh into the aluminum DSC sample pan. D-(+)-trehalose dihydrate (Sigma Life Sciences) was added to a DSC pan as-received.

RESULTS AND DISCUSSION

SDSC of urea crystals

Initial proof of concept studies for SDSC were performed using urea, which undergoes a simple single-stage solid/liquid phase transformation. **Figure 2A** shows the DSC trace for the melting transition of a urea sample (black line) overlaid with vertical lines corresponding to the normalized SHG areas of individual particles dropping below a threshold of 0.1 (view **Figure S1** for the overlay of the DSC trace and the full traces

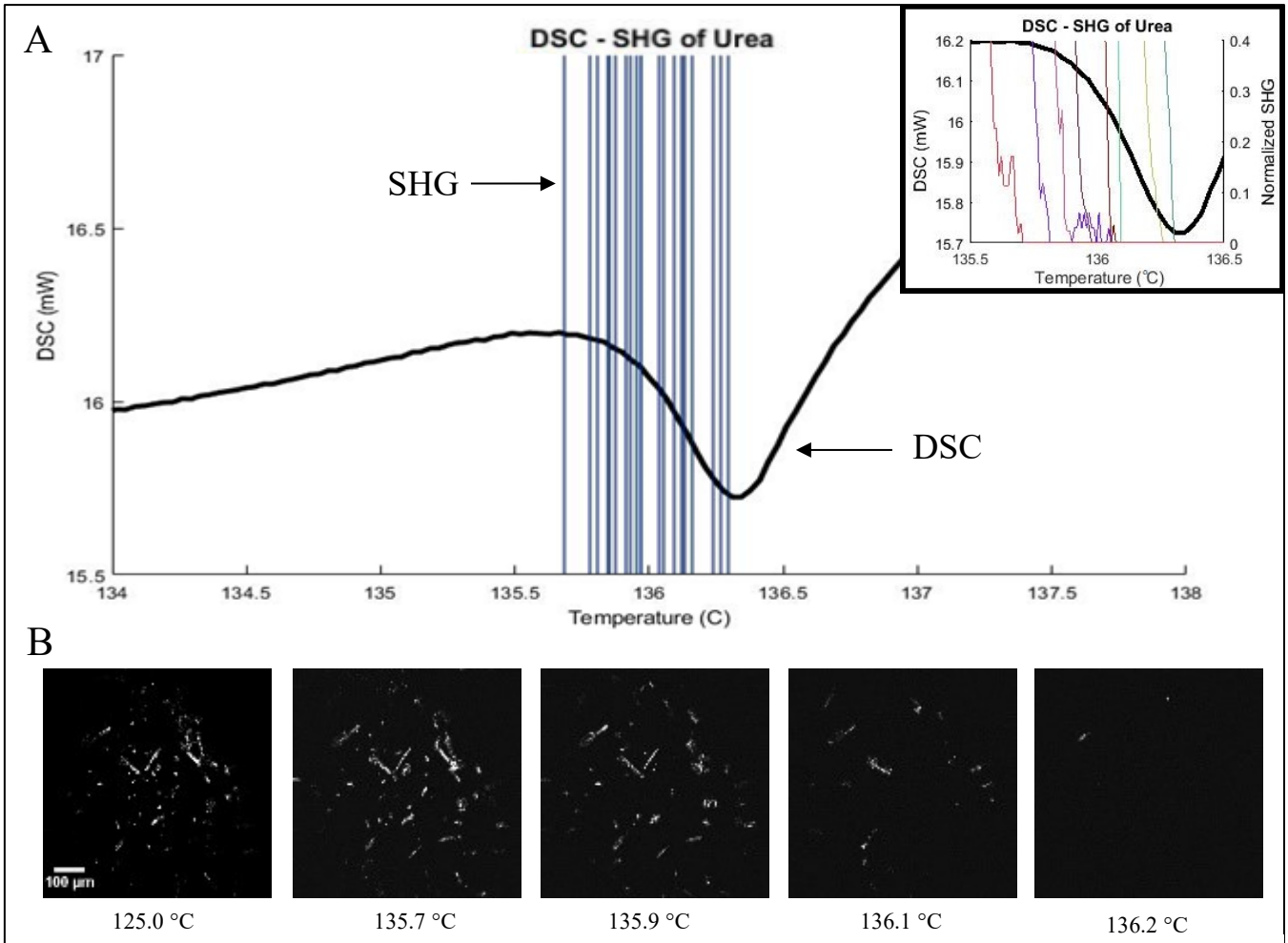

Figure 2. A) SDSC analysis of urea by combined SHG microscopy and DSC. The solid black line is the DSC trace of the melting of urea with endothermic direction being down (left-axis). The vertical colored lines show the temperatures in which the normalized SHG intensity of individual urea particles (acquired concurrently with DSC measurements) drops below a value of 0.1. DSC and SHG measurements both indicate a structural transformation in the same temperature range. The inset shows a zoom-in of the temperature range 135.5–136.5 °C where the color lines correspond to the normalized SHG intensity of individual urea particles. **B)** SHG microscope images of urea crystals during SDCS analysis. SHG microscopy reveals the stochastic nature of the melting transition and enables analysis on a per-particle basis.

of the normalized SHG areas of each particle).

The DSC trace indicates that the melting transition occurred at ~135 °C. This temperature is slightly higher than the literature value of 133 °C. This difference is attributed to a non-negligible heat transfer time to the sample. The need for optical access required the use of an unencapsulated sample pan, resulting in slower heat transfer.[35] Despite some baseline drift in the per-particle SHG activity from particle motion (view the combined SDSC video of urea in **Figure S2**), the single-particle SHG area shows much sharper transitions from the SHG-active crystalline form to the SHG-inactive molten liquid of urea indicated by the DSC trace, consistent with independent, stochastic melting events. Single-particle analysis yields a mean phase transition duration of 1.0 ± 0.6 s/particle while the DSC melting peak has a full-width-half-maximum of 3.3 s. This difference indicates that the rate of phase transformation was dictated largely by the rate for seed formation of the liquid-state within individual particles, followed by rapid phase transformation within a given particle. **Figure 2B** shows representative frames from a video acquired with the SHG microscope during the melting of urea (view the combined SDSC video of urea in **Figure S2**). From the SHG results, the nucleation rate at the phase transformation temperature can be estimated. In this work, a nucleation event is defined as the phase transformation of a single crystal (in this case, from solid to liquid). Nucleation rates were determined from the loss rate of SHG-active particles, measured as the intensity of each crystal decreased below a threshold (close to zero). Approximations for the per-particle mass using the density of urea and volume estimated from particle cross-sectional area yields a peak nucleation rate of $1.6 \pm 0.2 \times 10^4$ nuclei per second per milligram (based on the observed rate of 6.13 nuclei/s in a FoV with an estimated 0.39 µg of particulate mass; standard deviation was determined based on Poisson statistics for the number of crystals within the FoV). See **Figure S3** for the distribution of

crystal volumes and a description of the use of Poisson statistics for obtaining the uncertainty in the nucleation rate.

Consistent with numerous previous DSC studies of powders, SDSC measurements were performed exclusively as the temperature was increased to interrogate phase transformations.[36, 37] While in principle, additional information can be obtained from measurements of thermal events upon cooling, the phase transformations induced by heating were generally not easily reversible (e.g., dehydration). Even in the absence of composition changes, melting of many individual isolated particles results in coalescence to a homogeneous melt, while the reverse process will not recover isolated crystalline particles upon cooling. Furthermore, SDSC measurements upon cooling are complicated in practice by wicking of the liquid, which moves much of the sample out of the field of view. Although not the focus of the present study, it is worth noting that SHG microscopy has a rich history of informing on crystallization kinetics in accelerated stability assessments for active pharmaceutical ingredients.[38]

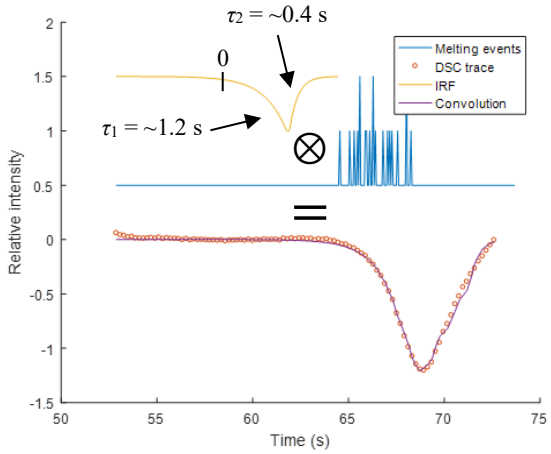

Figure 3. Comparison of the experimental DSC trace and the DSC trace generated from melting events. The best-fit double-exponential IRF (yellow) is convolved with impulsive melting events (blue) of single-particles observed in SHG images to generate the purple trace, which is in good agreement with the experimental DSC data (red). The time constant and offset of double-exponential IRF were optimized to minimize difference between experimental and generated DSC traces. Best-fit values of 1.161 ± 0.019 s, 0.435 ± 0.013 s, and 3.088 ± 0.013 s were computed for the double-exponential time constants and the offset respectively.

IRF determination with SDSC

The simultaneous SHG measurements were also used to determine the impulse response function (IRF) of the DSC instrument. As described in a preceding paragraph, the thermal events induced in the sample produced an instrument response with a temporal delay associated with heat transfer times. The macroscopic DSC endotherm arose from the net collective contributions from many such stochastic events. As such, the DSC observables were given by the convolution of the impulsive phase transformations with the IRF of the DSC system. Assuming a double-exponential IRF consistent with heat flow through a thermal resistor, the measured set of impulsive phase transformations by SHG $\boldsymbol{x}$ can be combined with the recorded DSC trace $\boldsymbol{y}$ to recover the maximum likelihood estimate (MLE) for the impulse response function $\hat{f}_{IRF} = f_{IRf}\left(\hat{\boldsymbol{a}}\right)$ described by the set of parameters $\boldsymbol{a}$ through $\hat{\boldsymbol{a}} = \arg\min_{\boldsymbol{a}} \left\| \boldsymbol{y} - \boldsymbol{x} \otimes f_{IRF}\left(\boldsymbol{a}\right) \right\|^2$. The results of an MLE fit of the measured DSC transient using the single-crystal phase transformation data from SHG is shown in **Figure 3**, recovering a phase-lag of 3.088 ± 0.013 s and rising and falling exponential time constants of 1.161 ± 0.019 s and 0.435 ± 0.013 s, respectively, for the double-exponential IRF. (See **Equations S1-S3** for a more detailed description of the least-squares fit to recover the IRF of the DSC instrument.) The phase-lag between the DSC event and the mean of the SHG events is attributed to delays from diffusive heat transfer from the individual particles to the pan and sample mount of the DSC instrument. The two time constants are tentatively attributed to the thermal diffusion times from the sample to the sample stage, and from the stage to the heat sink.[39] Even in a relatively simple melting transition, SHG provides the capability of mapping phase transformations on individual particles with temporal resolution much faster than achievable from conventional ensemble-averaged DSC measurements. The pairing of both methods provides information inaccessible by DSC alone; namely, that phase transformation proceeds through slow nucleation followed by rapid growth on a per particle basis with an intrinsic rate of 1.0 ± 0.6 s/particle (variance is dominated by particle-to-particle stochastics).

SDSC of trehalose dihydrate crystals

The performance of SDSC using the integrated SHG-DSC microscope was further tested with trehalose dihydrate, a molecule with complex phase behavior, including the existence of multiple transient crystal forms accessible under varying conditions.[40-43] Since significant differences in crystal structure can exist between polymorphs, hydrates, and solvates, SHG has the potential to aid in distinguishing transitions due to its sensitivity to noncentrosymmetric crystal forms.[23] **Figure 4** summarizes the SDSC analysis of trehalose dihydrate. Each colored line represents the percentage of pixels in an individual trehalose crystalline particle that exceeds a threshold. Four individual particles were monitored in this study. The black line is the DSC curve, in which dips correspond to endothermic events. For the temperature range of 140–220 °C, the collected SDSC images were summed and the logarithm of this summed image was cropped to the measured region of each particle. Each of the cropped images points to their representative SHG trace (the full FoV of the summed images can be seen in **Figure S4**).

DSC and SHG data were interpreted using previously reported literature values to map the polymorphic transitions of the sample through the temperature ramp. At the initial 80 °C, the weak SHG signal arises from the trehalose dihydrate (T_h) form that was initially added to the DSC pan before the temperature ramp.[44] The composition of this starting material was confirmed by powder X-ray diffraction (pXRD) to be primarily composed Th, although the unstable anhydrous form (T_α) may also be present at trace levels; previous reports indicate observation of the T_α form following room temperature storage at low relative humidity. The first signs of phase transformation activity occurred in the temperature range of 80–130 °C. The DSC curve exhibits a major endothermic peak in this

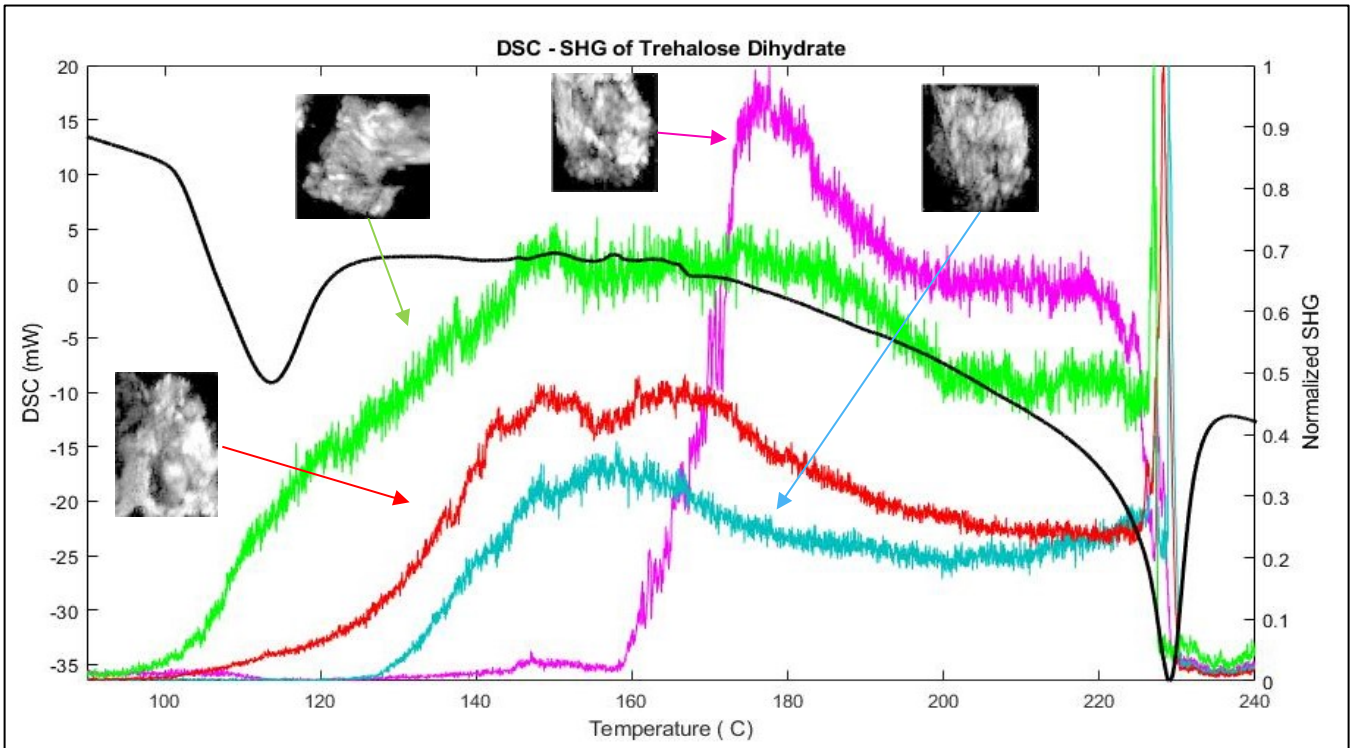

Figure 4. SDSC analysis of trehalose by SHG microscopy. The colored lines show the percentage of pixels in a trehalose particle above an SHG intensity threshold overlaid with the black line of the DSC trace with the endothermic direction being down. SDSC images were summed for the temperature range of 140–220 ºC and the logarithm of the summed image was cropped to the measured region of each particle (each cropped image points to the representative SHG trace).

range. This peak was previously reported to be the result of the dehydration of T_h.[36] Additionally, two distinct trends appear in the individual particle SHG data. Three of the trehalose particles increased in SHG activity while the other particle decreased over this same lower temperature range. The disparity in SHG activity between individual particles can be explained by the two major dehydration pathways available for T_h in this temperature range; T_h can either partially dehydrate with rearrangement to the crystalline T_γ form or completely dehydrate to an amorphous form (T_{am}).[36, 44] Similarly, the T_α form can also transition to the T_{am} form upon heating.[36, 37, 44, 45] The T_γ polymorph is theorized to be a mixture of T_h encapsulated in a shell of the crystalline, anhydrous form (T_β), which is SHG-active.[36, 45] Therefore, we conclude that the three particles that increased in SHG area in this temperature range likely transitioned to the SHG-active T_γ form, while the particle that reduced in SHG activity likely transitioned to the SHG-inactive T_{am} form at ~110 °C from either the T_h or T_{am} form.

The SHG activity generally increased for individual particles over the subsequent temperature range of 130–160 °C. The DSC curve exhibited small but reproducible features in this temperature range, the magnitude of which varies between experiments, and has been reported to be due to the dehydration of T_h.[36] Measurements of the fraction of SHG-active pixels in individual particles show that the three particles that previously exhibited SHG signal continue to convert over this temperature range. This increase in highly SHG-active fraction can simply be attributed to crystal growth over this temperature range. The fourth particle that previously decreased in SHG area shows a sharp increase in SHG area starting at ~160°C. SHG-inactive T_{am} has been previously reported to transition to SHG-active T_β in the range of 150–200 °C.[36, 44] Likewise, the T_α form has been reported to be able to transition directly to the T_β when held at a temperature of ~150 °C.[36, 37, 44, 45] However, this T_α transition has not been observed with the faster heating rates (20 °C/min.) used in the present study. Therefore, we conclude that this polymorphic transition from T_{am} to T_β is likely the cause of the sharp peak in SHG from the particle represented by the magenta trace.

Following the monotonic increases in transitioning to the T_β form from 130–160 °C, decreases in SHG were observed for all four particles in the range 160–200 °C. No peaks are observed in the DSC curve in this range, but the trehalose particles exhibit slowly varying and inhomogeneous loss in SHG activity. Several possible mechanisms for this loss in SHG activity were considered, two of which are described in detail. One possible explanation for loss in SHG activity with large crystal-to-crystal variability may be from interference effects as crystal sizes change during phase transformation.[46] Interference fringes from single crystals were reported previously in SHG microscopy measurements. However, interference effects were deemed unlikely for three reasons: i) interference effects would be anticipated to produce increases or decreases in SHG activity with equal probability, while only decays were observed experimentally, ii) the backwards coherence length is short (~100 nm) relative to the sizes of the crystals,

such that average activities would be expected, and iii) the interference is expected to vary with thickness, such that crystals with variance in dimensions would likely produces fringes over which the intensities are integrated. Alternatively, the decay in SHG signal can be explained by condensation of water vapor released by T_h onto the optical window of the DSC. Condensation was commonly seen in our experiments when working with hydrated samples because open crucible pans were used in the experiment to allow for imaging during DSC scans. Additionally, no purge gas was used to remove water vapor from the system, as addition of purge gas introduced measurement variance in the DSC analyses from variable heat transfer to the bath gas. Previously reported results by TGA indicate gradual water loss up to 200 ˚C,[36] consistent with the observed reduction in SHG signal that is proposed to arise from scattering losses from condensation. Furthermore, condensation is likely to impact some locations within the FoV to a greater extent than others, potentially providing an explanation for the large crystal-to-crystal variability in the loss. Thus, condensation is predicted to be the main cause of this loss in SHG signal.

Following the slow SHG signal loss from condensation, dramatic changes in the SHG-activity arose from 200–240 °C. In this range the DSC curve exhibited an endothermic peak at ~230 °C, and the SHG data displayed a sharp increase and subsequent decrease during the DSC peak (view the SDSC video of trehalose dihydrate in **Figure S5**). It is clear from the literature that the endothermic DSC peak arises from a melting transition.[36, 45] The final fall in SHG area is attributed to this melting event. However, the source of the sharp increase in SHG area prior to the melt has no precedent in reported DSC measurements. Two origins for the transient SHG area increase were considered.

First, significant mobility in the sample arose during the melting transition, which could alter the positions of the sample crystals relative to the focal plane. Crystals moving into the focal plane could result in an increase in SHG area, as SHG intensity scales with the squared power of incident light. Second, the increase could be explained by a change in the crystal form, degree of crystallinity, or crystal size of trehalose. To evaluate the first mechanism, a custom optic, designed in-house, was added to the beam path to extend the depth-of-field from ~20 μm to ~100 μm (detailed in a manuscript in preparation). The sharp peak in SHG prior to the melt was still observed while imaging with an extended depth-of-field, suggesting that crystal movement into the focal volume is not likely to be the major cause of the increase in SHG area.

Alternatively, the increase in SHG area could arise from a change in the crystal form, degree of crystallinity, or crystal size of trehalose. While it is possible that there exists a previously unknown polymorphic transition immediately prior to the melt of trehalose, this possibility was rejected on the principal of Occam's razor, in light of the extensive body of prior work done to characterize the polymorphism of trehalose. A more plausible origin for the spike in SHG area is from the final conversion of the remaining T_h core of T_γ polymorph to T_β, promoted by an increase in the energy in molecular diffusion immediately prior to the melting transition. Additionally, another closely related contribution to the increase in SHG area could be the rapid growth of T_β crystalline domains of trehalose from residual T_{am} due to increase mobility immediately prior to the melt. In summary, the particles observed in this study are theorized to undergo one of two general phase transition pathways: $T_h \rightarrow T_{am} \rightarrow T_\beta \rightarrow$ melt or $T_h \rightarrow T_\gamma \rightarrow T_\beta \rightarrow$ melt.

Notably, this "cold phase transformation" phenomenon, in which phase transformation to the SHG-active crystalline form occurs immediately prior to the transition to the liquid form, was clearly observable by SHG but undetectable in the DSC measurements. This latter proposed mechanism has precedent in observations of "cold crystallization" in DSC, in which transient crystallization arises upon transformation from a glassy state to a liquid.[47] In DSC, cold crystallization appears as an exothermic peak immediately preceding an endothermic peak. Cold crystallization has been observed in studies of T_h for the transition from a glassy material to the T_β form.[45] However, to our knowledge, this study represents the first observation of cold transformation between two different solid-state crystalline forms prior to the melt. Importantly, evidence supporting cold transformation was undetectable by DSC alone, presumably obfuscated by the comparatively longer response time and inherent ensemble averaging associated with the DSC measurements.

As discussed before, the reversibility of the SDSC was not investigated for trehalose dihydrate. Like the urea samples, wetting of the sample pan after heating of the sample presented challenges in maintaining sample position within the field of view following the melt. Likewise, reversibility after dehydration (< 220ºC) would not be anticipated due to the large entropic barriers involved with rehydration of the sample under high humidity. Studies have shown that the dehydrated sample can rehydrate to the original material, but over timescales significantly longer than easily accessible by DSC.[48, 49]

Analysis of the impulse response function from urea provides a route for connecting the cold phase transformation and melting processes to the DSC endotherm at ~230 ºC. The entire transformation to produce the SHG-active crystal form, followed by melting progressed all within ~2 seconds, likely explaining the absence of prior work describing cold phase transformation. **Figure S6** shows the results of the convolution of the IRF determined from the urea analysis, with impulses corresponding to either the initial rise from the "cold phase transformation" or the melt. Neither of the resulting curves coincides directly with that of the DSC melting peak. This disparity likely arises from the statistics of small numbers, as only four particles in the FoV were available for analysis (as opposed to 58 crystals for urea).

Differences between single-particle and ensemble-averaged measurements are particularly noteworthy in the results shown in **Figure 4**. The integrated SHG intensity from one particular crystal indicated bv the green trace nicely tracks the DSC trace and is likely to be representative of the major ensemble-averaged thermal event at ~110 ºC. However, it is clear that distinctly different phase transformation behaviors are observed within a subset of the population, exemplified by the red, cyan, and purple traces. This apparent incongruency is attributed to the stochastic nature of the sample, with multiple thermally accessible transformation pathways available.

Trehalose dihydrate has multiple competing pathways to various crystal forms, which are stochastically accessed over large temperature ranges and which are likely to produce significantly different heats of phase transformation. This rich landscape of crystal form space is largely obscured by ensemble-averaged measurements of DSC alone, but is clearly accessed by per-particle analysis using SHG microscopy.

CONCLUSIONS

SDSC was shown to enable connection of internal structural rearrangements within crystalline materials measured by SHG on single particles to the heat flow recorded by DSC. SHG measurements were sensitive to variations in the molecular packing arrangements during the phase transitions of individual particles that are generally inaccessible in conventional microscopy. Coupling the structural data acquired from SHG imaging with DSC enabled single-particle measurements disentangled from the ensemble-averaged thermal transients recorded with DSC. A proof-of-concept SDSC experiment was performed on urea, which has a single solid/liquid phase transformation. From these measurements, the IRF of the DSC system was determined, showing that the melt proceeds through a slow nucleation step followed by rapid growth on a per particle basis. Next, SDSC was used to characterize the phase behavior of a more complex system, trehalose dihydrate. The dehydration events of trehalose dihydrate were readily observed by SDSC and the higher temporal resolution of SHG measurements, compared to that of the temporal resolution of typical DSC measurements, allowed for detection of a rapid phase transformation not observable by DSC. Thus, SDSC is proposed as a novel technique for the pharmaceutical drug development pipeline for the characterization of single-particle phase transformations.

ASSOCIATED CONTENT

Supporting Information

Supporting Information (PDF)
Figure S2 SDSC Video of Urea (AVI)
Figure S5 SDSC Video of Trehalose Dihydrate (AVI)

AUTHOR INFORMATION

Corresponding Author

*Email: gsimpson@purdue.edu

Notes

The authors declare no competing financial interest.

ACKNOWLEDGMENT

The authors would like to acknowledge the support from Eli Lilly and Company through the Lilly Research Awards Program (LRAP), grant #209682 and the NSF-GOALI Grant No. CHE-1710475.

REFERENCES

1. Strovel, J.; Sittampalam, S.; Coussens, N. P.; Hughes, M.; Inglese, J.; Kurtz, A.; Andalibi, A.; Patton, L.; Austin, C.; Baltezor, M., Early drug discovery and development guidelines: for academic researchers, collaborators, and start-up companies. **2016**.
2. Cheney, M. L.; Shan, N.; Healey, E. R.; Hanna, M.; Wojtas, L.; Zaworotko, M. J.; Sava, V.; Song, S.; Sanchez-Ramos, J. R., Effects of crystal form on solubility and pharmacokinetics: a crystal engineering case study of lamotrigine. *Crystal Growth & Design* **2009,** *10* (1), 394-405.
3. Maddileti, D.; Swapna, B.; Nangia, A., High solubility crystalline pharmaceutical Forms of blonanserin. *Crystal Growth & Design* **2014,** *14* (5), 2557-2570.
4. Yadav, A.; Shete, A.; Dabke, A.; Kulkarni, P.; Sakhare, S., Co-crystals: a novel approach to modify physicochemical properties of active pharmaceutical ingredients. *Indian journal of pharmaceutical sciences* **2009,** *71* (4), 359.
5. Newman, A.; Knipp, G.; Zografi, G., Assessing the performance of amorphous solid dispersions. *Journal of pharmaceutical sciences* **2012,** *101* (4), 1355-1377.
6. Baghel, S.; Cathcart, H.; O'Reilly, N. J., Polymeric amorphous solid dispersions: a review of amorphization, crystallization, stabilization, solid-state characterization, and aqueous solubilization of biopharmaceutical classification system class II drugs. *Journal of pharmaceutical sciences* **2016,** *105* (9), 2527-2544.
7. Jackson, M. J.; Kestur, U. S.; Hussain, M. A.; Taylor, L. S., Dissolution of danazol amorphous solid dispersions: supersaturation and phase behavior as a function of drug loading and polymer type. *Molecular pharmaceutics* **2015,** *13* (1), 223-231.
8. Konno, H.; Taylor, L. S., Ability of different polymers to inhibit the crystallization of amorphous felodipine in the presence of moisture. *Pharmaceutical research* **2008,** *25* (4), 969-978.
9. Shamblin, S. L.; Zografi, G., The effects of absorbed water on the properties of amorphous mixtures containing sucrose. *Pharmaceutical research* **1999,** *16* (7), 1119-1124.
10. Andronis, V.; Yoshioka, M.; Zografi, G., Effects of sorbed water on the crystallization of indomethacin from the amorphous state. *Journal of pharmaceutical sciences* **1997,** *86* (3), 346-351.
11. Rumondor, A. C.; Stanford, L. A.; Taylor, L. S., Effects of polymer type and storage relative humidity on the kinetics of felodipine crystallization from amorphous solid dispersions. *Pharmaceutical research* **2009,** *26* (12), 2599.
12. Clas, S.-D.; Dalton, C. R.; Hancock, B. C., Differential scanning calorimetry: applications in drug development. *Pharmaceutical science & technology today* **1999,** *2* (8), 311-320.
13. Oxtoby, D. W., Nucleation of first-order phase transitions. *Accounts of chemical research* **1998,** *31* (2), 91-97.
14. Khaliullin, R. Z.; Eshet, H.; Kühne, T. D.; Behler, J.; Parrinello, M., Nucleation mechanism for the direct graphite-to-diamond phase transition. *Nature materials* **2011,** *10* (9), 693.
15. Sleutel, M.; Lutsko, J.; Van Driessche, A. E.; Durán-Olivencia, M. A.; Maes, D., Observing classical nucleation theory at work by monitoring phase transitions with molecular precision. *Nature communications* **2014,** *5*, 5598.
16. Liu, H.; Kwon, O.-H.; Tang, J.; Zewail, A. H., 4D imaging and diffraction dynamics of single-particle phase transition in heterogeneous ensembles. *Nano letters* **2014,** *14* (2), 946-954.
17. Reading, M., Thermal Analysis by Structural Characterization (TASC): Structural and Thermo-Rheological Information from Hot Stage Microscopy. *Microscopy Today* **2017,** *25* (5), 18-23.
18. Reading, M.; Morton, M.; Antonijevic, M.; Grandy, D.; Hourston, D.; Lacey, A., New methods of thermal analysis and chemical mapping on a micro and nano scale by combining microscopy with image analysis. *Microscopy: advances in scientific research and education. Formatex Research Center* **2014**, 1083-9.
19. Alhijjaj, M.; Belton, P.; Fabian, L.; Wellner, N.; Reading, M.; Qi, S., Novel Thermal Imaging Method for Rapid Screening of Drug–Polymer Miscibility for Solid Dispersion Based Formulation Development. *Molecular pharmaceutics* **2018,** *15* (12), 5625-5636.
20. Alhijjaj, M.; Reading, M.; Belton, P.; Qi, S., Thermal analysis by structural characterization as a method for assessing heterogeneity in complex solid pharmaceutical dosage forms. *Analytical chemistry* **2015,** *87* (21), 10848-10855.
21. Alhijjaj, M.; Yassin, S.; Reading, M.; Zeitler, J. A.; Belton, P.; Qi, S., Characterization of heterogeneity and spatial distribution of phases in complex solid dispersions by thermal analysis by structural characterization and X-ray micro computed tomography. *Pharmaceutical research* **2017,** *34* (5), 971-989.
22. Kestur, U. S.; Wanapun, D.; Toth, S. J.; Wegiel, L. A.; Simpson, G. J.; Taylor, L. S., Nonlinear optical imaging for sensitive detection of crystals in bulk amorphous powders. *Journal of pharmaceutical sciences* **2012,** *101* (11), 4201-4213.
23. Chowdhury, A. U.; Dettmar, C. M.; Sullivan, S. Z.; Zhang, S.; Jacobs, K. T.; Kissick, D. J.; Maltais, T.; Hedderich, H. G.; Bishop, P. A.; Simpson, G. J., Kinetic trapping of metastable amino acid polymorphs. *J. Am. Chem. Soc.* **2014,** *136* (6), 2404-2412.
24. Smith, C. J.; Dinh, J.; Schmitt, P. D.; Stroud, P. A.; Hinds, J.; Johnson, M.; Simpson, G., EXPRESS: Calibration-Free Second Harmonic Generation (SHG) Image Analysis for Quantification of Trace Crystallinity within Final Dosage Forms of Amorphous Solid Dispersions. *Applied spectroscopy* **2018**, 0003702818786506.
25. Scarborough, N. M.; Godaliyadda, G.; Ye, D. H.; Kissick, D. J.; Zhang, S.; Newman, J. A.; Sheedlo, M. J.; Chowdhury, A.; Fischetti, R.

F.; Das, C., Synchrotron X-Ray Diffraction Dynamic Sampling for Protein Crystal Centering. *Electronic Imaging* **2017,** *2017* (17), 6-9.
26. Simon, F.; Clevers, S.; Dupray, V.; Coquerel, G., Relevance of the second harmonic generation to characterize crystalline samples. *Chemical Engineering & Technology* **2015,** *38* (6), 971-983.
27. Galland, A.; Dupray, V.; Berton, B.; Morin-Grognet, S.; Sanselme, M.; Atmani, H.; Coquerel, G., Spotting conglomerates by second harmonic generation. *Crystal Growth and Design* **2009,** *9* (6), 2713-2718.
28. Francis, A. T.; Nguyen, T. T.; Lamm, M. S.; Teller, R.; Forster, S. P.; Xu, W.; Rhodes, T.; Smith, R. L.; Kuiper, J.; Su, Y., In Situ Stimulated Raman Scattering (SRS) Microscopy Study of the Dissolution of Sustained-Release Implant Formulation. *Molecular pharmaceutics* **2018,** *15* (12), 5793-5801.
29. Heinz, A.; Strachan, C. J.; Gordon, K. C.; Rades, T., Analysis of solid-state transformations of pharmaceutical compounds using vibrational spectroscopy. *Journal of Pharmacy and Pharmacology* **2009,** *61* (8), 971-988.
30. Zeitler, J. A.; Kogermann, K.; Rantanen, J.; Rades, T.; Taday, P. F.; Pepper, M.; Aaltonen, J.; Strachan, C. J., Drug hydrate systems and dehydration processes studied by terahertz pulsed spectroscopy. *International journal of pharmaceutics* **2007,** *334* (1-2), 78-84.
31. Zeitler, J. A.; Newnham, D. A.; Taday, P. F.; Threlfall, T. L.; Lancaster, R. W.; Berg, R. W.; Strachan, C. J.; Pepper, M.; Gordon, K. C.; Rades, T., Characterization of temperature-induced phase transitions in five polymorphic forms of sulfathiazole by terahertz pulsed spectroscopy and differential scanning calorimetry. *Journal of pharmaceutical sciences* **2006,** *95* (11), 2486-2498.
32. Strachan, C. J.; Rades, T.; Gordon, K. C.; Rantanen, J., Raman spectroscopy for quantitative analysis of pharmaceutical solids. *Journal of pharmacy and pharmacology* **2007,** *59* (2), 179-192.
33. Strachan, C. J.; Taday, P. F.; Newnham, D. A.; Gordon, K. C.; Zeitler, J. A.; Pepper, M.; Rades, T., Using terahertz pulsed spectroscopy to quantify pharmaceutical polymorphism and crystallinity. *Journal of Pharmaceutical Sciences* **2005,** *94* (4), 837-846.
34. Muir, R. D.; Sullivan, S. Z.; Oglesbee, R. A.; Simpson, G. J., Synchronous digitization for high dynamic range lock-in amplification in beam-scanning microscopy. *Review of Scientific Instruments* **2014,** *85* (3), 033703.
35. Gaisford, S.; Kett, V.; Haines, P., *Principles of thermal analysis and calorimetry*. Royal society of chemistry: 2016.
36. Raimi-Abraham, B. T.; Moffat, J. G.; Belton, P. S.; Barker, S. A.; Craig, D. Q. M., Generation and Characterization of Standardized Forms of Trehalose Dihydrate and Their Associated Solid-State Behavior. *Crystal Growth & Design* **2014,** *14* (10), 4955-4967.
37. Rani, M.; Govindarajan, R.; Surana, R.; Suryanarayanan, R., Structure in dehydrated trehalose dihydrate - Evaluation of the concept of partial crystallinity. *Pharmaceutical Research* **2006,** *23* (10), 2356-2367.
38. Song, Z. T.; Sarkar, S.; Vogt, A. D.; Danzer, G. D.; Smith, C. J.; Gualtier, E. J.; Simpson, G. J., Kinetic Modeling of Accelerated Stability Testing Enabled by Second Harmonic Generation Microscopy. *Analytical Chemistry* **2018,** *90* (7), 4406-4413.
39. Höhne, G. W. H.; Hemminger, W.; Flammersheim, H.-J., Theoretical fundamentals of differential scanning calorimeters. In *Differential Scanning Calorimetry*, Springer: 1996; pp 21-40.
40. Singh, S. K., Sucrose and Trehalose in Therapeutic Protein Formulations. In *Challenges in Protein Product Development*, Springer: 2018; pp 63-95.
41. Taylor, L. S.; Williams, A. C.; York, P., Particle size dependent molecular rearrangements during the dehydration of trehalose dihydrate-in situ FT-Raman spectroscopy. *Pharmaceutical research* **1998,** *15* (8), 1207-1214.
42. Taylor, L. S.; York, P., Effect of particle size and temperature on the dehydration kinetics of trehalose dihydrate. *International journal of pharmaceutics* **1998,** *167* (1-2), 215-221.
43. Taylor, L. S.; York, P., Characterization of the phase transitions of trehalose dihydrate on heating and subsequent dehydration. *Journal of pharmaceutical sciences* **1998,** *87* (3), 347-355.
44. Sussich, F.; Urbani, R.; Princivalle, F.; Cesaro, A., Polymorphic amorphous and crystalline forms of trehalose. *Journal of the American Chemical Society* **1998,** *120* (31), 7893-7899.
45. Sussich, F.; Princivalle, F.; Cesàro, A., The interplay of the rate of water removal in the dehydration of α, α-trehalose. *Carbohydrate research* **1999,** *322* (1-2), 113-119.
46. Dow, X. Y.; DeWalt, E. L.; Sullivan, S. Z.; Schmitt, P. D.; Ulcickas, J. R.; Simpson, G. J., Imaging the nonlinear susceptibility tensor of collagen by nonlinear optical stokes ellipsometry. *Biophysical journal* **2016,** *111* (7), 1361-1374.
47. Wunderlich, B., Theory of cold crystallization of high polymers. *The Journal of Chemical Physics* **1958,** *29* (6), 1395-1404.
48. Furuki, T.; Kishi, A.; Sakurai, M., De- and rehydration behavior of alpha,alpha-trehalose dihydrate under humidity-controlled atmospheres. *Carbohydrate Research* **2005,** *340* (3), 429-438.
49. Jones, M. D.; Hooton, J. C.; Dawson, M. L.; Ferrie, A. R.; Price, R., Dehydration of trehalose dihydrate at low relative humidity and ambient temperature. *International Journal of Pharmaceutics* **2006,** *313* (1-2), 87-98.

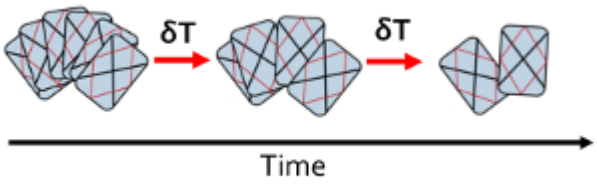

For Table of Contents Only.